Performance analysis of an integrated piezoelectric ZnO sensor for detection of head–disk contact

Yuan, Yanhui; Du, Hejun; Chow, Kun Shyong; Zhang, Mingsheng; Yu, Shengkai; Liu, Bo

2013

Yuan, Y., Du, H., Chow, K. S., Zhang, M., Yu, S., & Liu, B. (2013). Performance analysis of an integrated piezoelectric ZnO sensor for detection of head–disk contact. Microsystem Technologies, 19(9-10), 1449-1455.

https://hdl.handle.net/10356/101400

https://doi.org/10.1007/s00542-013-1839-3

Performance analysis of an integrated piezoelectric ZnO sensor for detection of head-disk contact

Yanhui Yuan[1], Hejun Du[1,] *, Kun Shyong Chow[1], Mingsheng Zhang[2], Shengkai Yu[2], Bo Liu[2]

[1]*School of Mechanical and Aerospace Engineering, Nanyang Technological University, 50 Nanyang Avenue, Singapore, 639798, Singapore*

[2]*Data Storage Institute, Engineering Drive 1, 117608, Singapore*

* Corresponding author. Email address: mhdu@ntu.edu.sg; Tel: +65 6790 4783; Fax: +65 6790 4783.

Abstract

Integrated capability for detection of head-disk contact is desired for magnetic sliders with near-contact flying height. At the same time, fabrication of added features should be compatible with the existing slider micromachining process which is highly specialized and cost sensitive. Aimed at meeting the two requirements, a novel sensor configuration is explored in the present study. The new sensor configuration consists of a piezoelectric zinc oxide (ZnO) thin-film sensor sandwiched in the magnetic slider on its trailing side. Coupled structural and piezoelectric finite-element analysis for a sensor-slider- suspension assembly was performed to investigate the dynamic sensing performance. Output voltages on the millivolt level were obtained under typical head-disk interactions. The 2nd in-plane bending mode of the slider was found to be the major contributor to the output voltage. Parametric study showed that a thicker ZnO layer generally generated a larger output, while the thickness of the slider overcoat only had minimal effect. Simulation results from harmonic and transient analyses demonstrated that the piezoelectric thin-film ZnO sensor is sufficiently sensitive for detection of head-disk contact.

1. Introduction

Head-disk contact becomes inevitable when flying height of the magnetic slider in the hard disk drive approaches sub-5 nanometer in order to achieve areal densities beyond 500 Gb/in^2 (Marchon and Olson 2009). Head-disk contact can cause damage to the head-disk interface (HDI) and read/write failure. Conventional piezoelectric acoustic emission (AE) sensors have been used for decades to monitor head-disk interactions (Kita et al. 1980; Yeack-Scranton 1986; Wang et al. 1998). AE sensors are usually placed on the actuator arm (Kohira et al. 2001) or the drive cover (Daugela et al. 2007). Elastic stress waves induced by head-disk contact propagate through the slider and suspension to the actuator arm and drive cover. AE sensors receive and convert the stress waves into electric charge by piezoelectric effect. Conventional AE sensors are a very effective tool for HDI characterization in a lab setting. However they cannot be used in the control servo for real-time flying height control, because conventional AE sensors and signal conditioning circuits are too bulky to be integrated into and shipped with the hard disk drive. In efforts to integrate a piezoelectric sensor into the hard disk drive, researchers (Imai et al. 1995; Imai et al. 1996) fabricated piezoelectric ZnO sensors on the top of the slider, parallel to the air bearing surface. Although their study demonstrated that thin-film piezoelectric sensors can be integrated into the slider, fabrication on the top surface of the slider is not compatible with the standard slider fabrication process (Naniwa et al. 2009). To enable process integration, additional thin-film sensors can be deposited only on the trailing side of the slider. However sensitivity of this new configuration can be compromised, as in vibration the top of the slider usually experiences more strain than the side. Therefore, feasibility of the new sensor configuration depends on whether it is

sensitive enough to generate an adequate signal. In our recent study (Shen et al. 2012), the static response of a piezoelectric ZnO sensor with the new configuration was simulated. Under a static force of 1 μN, output voltage of 0.1 mV was observed. The results were promising considering the dynamic head-disk contact force is usually on the level of millinewtons (Knigge and Talke 2000). The purpose of the present work is to further investigate the sensing capability of the piezoelectric ZnO sensor under dynamic head-disk contact. Harmonic and transient responses of the ZnO sensor have been obtained by finite element analysis. Dependence of its output on slider vibration modes as well as thicknesses of ZnO and overcoat has been analyzed.

2. Sensor operation principle

Due to surface roughness and waviness, the slider comes into intermittent contact with the disk (Fig. 1(a)). The contact force causes dynamic stress in the slider body. As shown in Fig. 1 (a) and (b), the ZnO sensor located beneath the slider overcoat detects the stress, thus the head-disk contact.

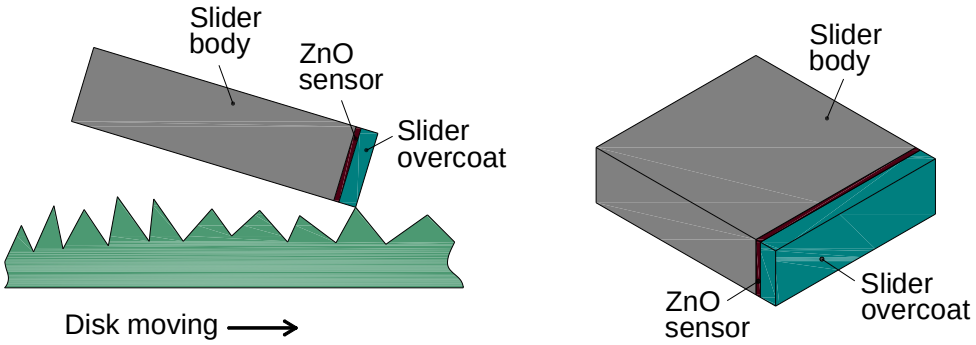

Fig. 1 (a) Slider in contact with disk; (b) slider with ZnO sensor

When a force is applied on a piezoelectric material, electric charge/voltage will be generated due to piezoelectric effect. A piezoelectric sensor can operate in either the d_{31} mode or d_{33} mode. In the d_{31} mode (Fig. 2(a)), the external force ΔF and

displacement ΔL are applied in a direction transverse to the polarization P, while in the d_{33} mode (Fig. 2(a)) the inputs (ΔF and ΔT) are parallel to the polarization P. Although the coupling coefficient d_{33} is usually larger than d_{31}, sensors based on the d_{33} mode do not necessarily outperform those based on the d_{31} mode. Apart from the coupling coefficients, the strength of the output signal also depends on the input, i.e. stress or strain. In structures, such as cantilever benders, strain occurs dominantly in the transverse direction, thus the d_{31} mode for this kind of structures is much more sensitive. In the sensor configuration of the present study (Fig. 1(b)), the d_{31} and d_{33} modes of the ZnO sensor respond to slider in-plane bending and compression, respectively. Under excitation of head-disk contact, the magnitude of slider bending is likely much larger than that of compression. As a result, the contact signal will be contributed mainly by the d_{31} mode.

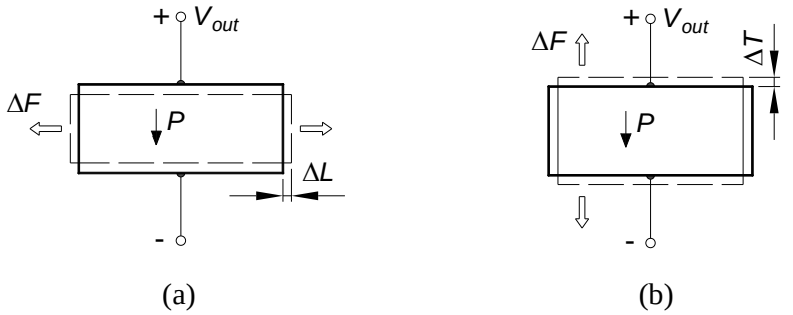

Fig. 2 Sensor operation mode: (a) d_{31} mode; (b) d_{33} mode

To understand slider vibration, a modal analysis was performed on the slider to identify its modal shapes and frequencies. The modal frequencies of the first ten modes are listed in Table 1. The 7th, 8th and 9th modes are identified as the first three in-plane bending modes (Figure 3). As shown in Fig. 3(a), the 1st in-plane bending mode is symmetrical about the slider mid-plane. The 2nd and 3rd in-plane bending modes are asymmetrical. In the 2nd in-plane bending mode (Fig. 3(b)), deformation occurs mainly at the trailing side, while in the 3rd in-plane bending mode (Fig. 3(c)), deformation shifts to the opposite (leading) side. Since the

Table 1 Slider vibration modes

Modal No.	1	2	3	4	5	6	7	8	9	10
Freq. (MHz)	1.73	2.22	3.32	3.64	4.15	4.77	5.15	5.52	5.97	6.18

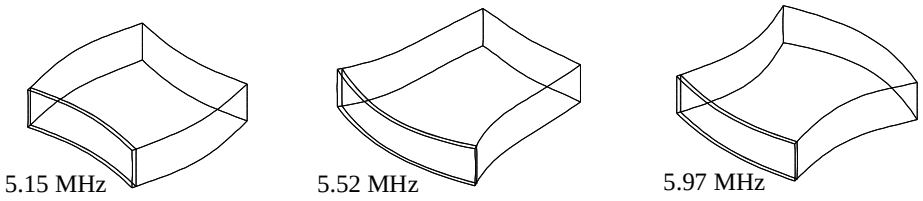

Fig. 3 Slider in-plane bending: (a) 1st mode; (b) 2nd mode; (c) 3rd mode

sensor is located at the trailing side, the 3rd mode is expected to contribute less to the sensor output than the 2nd mode. Direct excitation from the contact force on these three in-plane bending modes is minimal, because the contact force is perpendicular to the main slider planes. However, since the in-plane modes and other modes, such as torsion and out-of-plane bending, are coupled, in-plane bending can still be excited by the contact force through coupling. Their vibration amplitude can be much smaller than out-of-plane bending modes. Therefore piezoelectric sensors deployed on the top surface of the slider are more sensitive than the present configuration. As explained earlier in the literature review, the motivation behind this study is to provide a solution which is adequately sensitive and compatible with the slider fabrication process.

3. Finite element model

3.1 Finite element formulation

The electromechanical constitutive equations for linear material behavior are given in matrix form by (IEEE 1996)

$$\{\mathbf{T}\} = [\mathbf{c}]\{\mathbf{S}\} - [\mathbf{e}]\{\mathbf{E}\} \quad (1)$$

$$\{\mathbf{D}\} = [\mathbf{e}]^{\mathrm{T}}\{\mathbf{S}\} + [\boldsymbol{\varepsilon}]\{\mathbf{E}\} \quad (2)$$

where $\{\mathbf{T}\}$, $\{\mathbf{D}\}$, $\{\mathbf{S}\}$ and $\{\mathbf{E}\}$ are the stress vector, electric displacement field vector, strain vector, and electric field vector, respectively; $[\mathbf{c}]$, $[\mathbf{e}]$ and $[\boldsymbol{\varepsilon}]$ are the stiffness matrix evaluated at constant electric field, piezoelectric stress matrix and dielectric matrix evaluated at constant strain, respectively. Due to crystal symmetry of the ZnO wurtzite structure, there are only three nonzero independent components (e_{31}, e_{33}, and e_{15}) in the piezoelectric stress matrix $[\mathbf{e}]$ (Morkoç and Özgür 2009)

$$[\mathbf{e}]=\begin{bmatrix} 0 & 0 & 0 & 0 & e_{15} & 0 \\ 0 & 0 & 0 & e_{15} & 0 & 0 \\ e_{31} & e_{31} & e_{33} & 0 & 0 & 0 \end{bmatrix} \tag{3}$$

Similarly, the stiffness matrix [**c**] has only five independent constants (c_{11}, c_{12}, c_{13}, c_{33}, c_{44})

$$[\mathbf{c}]=\begin{bmatrix} c_{11} & c_{12} & c_{13} & & & \\ c_{12} & c_{11} & c_{13} & & & \\ c_{13} & c_{13} & c_{33} & & & \\ & & & c_{44} & & \\ & & & & c_{44} & \\ & & & & & (c_{11}-c_{12})/2 \end{bmatrix} \tag{4}$$

After the application of the variational principle and finite element discretization, the equations of motion for node *i*, are given by (Allik and Hughes 1970)

$$[\mathbf{m}]\{\ddot{\mathbf{u}}_i\}+[\mathbf{k}_{uu}]\{\mathbf{u}_i\}+[\mathbf{k}_{u\phi}]\{\boldsymbol{\phi}_i\}=\{\mathbf{F}_B\}+\{\mathbf{F}_S\}+\{\mathbf{F}_P\} \tag{5}$$

where $\{\mathbf{u}_i\}$, $\{\boldsymbol{\phi}_i\}$, $\{\mathbf{F}_B\}$, $\{\mathbf{F}_S\}$, and $\{\mathbf{F}_P\}$ denote vectors of displacement, electric potential, body force, surface force and concentrated force, respectively; [**m**], $[\mathbf{k}_{uu}]$, and $[\mathbf{k}_{u\phi}]$ denote matrices of mass, stiffness, and piezoelectric coupling, respectively. In addition to the equations of motion, the equilibrium equations for electric potential are

$$[\mathbf{k}_{u\phi}]^{\mathrm{T}}\{\mathbf{u}_i\}+[\mathbf{k}_{\phi\phi}]\{\boldsymbol{\phi}_i\}=\{\mathbf{Q}_B\}+\{\mathbf{Q}_S\}+\{\mathbf{Q}_P\} \tag{6}$$

where $\{\mathbf{Q}_B\}$, $\{\mathbf{Q}_S\}$, and $\{\mathbf{Q}_P\}$ are vectors of body charge, surface charge and point charge, respectively; $[\mathbf{k}_{\phi\phi}]$ is dielectric conductivity matrix. Once nodal displacement $\{\mathbf{u}_i\}$ and electric potential $\{\boldsymbol{\phi}_i\}$ are determined, strain {**S**} and electric field {**E**} can be obtained. Subsequently, stress {**T**} and electric displacement field {**D**} can be found from Eqs. 1 and 2.

3.2 Finite element model of sensor-slider-suspension assembly

Fig. 4(a) shows the finite element model of a pico-slider-suspension assembly created with the commercial finite-element-analysis software Ansys 10.0. The suspension, slider body and piezoelectric ZnO sensor were meshed with finite elements of SHELL63, SOLID45 and SOLID5, respectively. The air bearing is believed to have minimal effect on the sensor performance, as its frequencies are much lower than those of the slider. Therefore, for less complexity, the air bearing was simplified into three spring-damper systems (COMIN14). To simulate head-

disk contact, a normal force F_n is applied on the front pad of the slider as shown in Fig. 4(b). The material properties of the sensor -slider-suspension components are listed in Table 2 and Table 3.

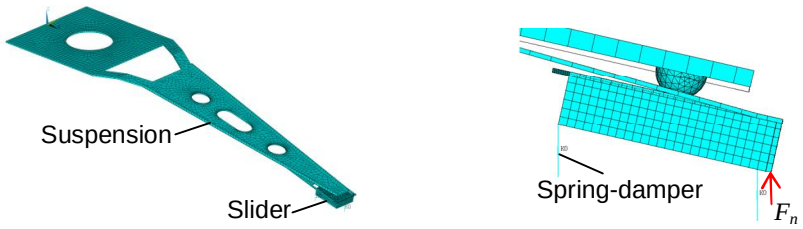

(a) (b)

Fig. 4 (a) Slider-suspension assembly; (b) simplified air bearing

Table 2 Material properties of slider-suspension components

Materials	Young's modulus (GPa)	Poisson's ratio	Density (kg/m^3)
Al_2O_3TiC (Slider body)	390	0.22	2200
Al_2O_3 (Slider overcoat)	138	0.25	2200
ZnO (Sensor)	N.A.	0.34	5750
Stainless steel (Suspension)	193	0.29	8000

Table 3 Piezoelectric and stiffness constants of ZnO (Jagadish and Pearton 2006)

Parameter	Value	Parameter	Value
c_{11} (GPa)	209.7	c_{44} (GPa)	42.47
c_{12} (GPa)	121.1	d_{31} (10^{-12} C/N)	-5.43
c_{13} (GPa)	105.1	d_{33} (10^{-12} C/N)	11.67
c_{33} (GPa)	210.9	d_{15} (10^{-12} C/N)	-11.34

In the simulation, the piezoelectric strain matrix [**d**] was used instead of the stiffness stress matrix [**c**], as it would be more convenient to study the contributions of d_{31} and d_{33} modes. The piezoelectric strain matrix [**d**] has the same form as the piezoelectric stress matrix [**c**]

$$[\mathbf{d}] = \begin{bmatrix} 0 & 0 & 0 & 0 & d_{15} & 0 \\ 0 & 0 & 0 & d_{15} & 0 & 0 \\ d_{31} & d_{31} & d_{33} & 0 & 0 & 0 \end{bmatrix} \quad (7)$$

The two matrices are related through the stiffness stress matrix [**c**]

$$[\mathbf{e}] = [\mathbf{d}][\mathbf{c}] \quad (8)$$

4. Harmonic analysis of sensor response

Coupled structural and piezoelectric analysis was performed for the suspension-slider-sensor assembly. (Knigge and Talke 2000)A harmonic force of 1mN was applied to the front pad of the slider as shown in Fig. 4(b). Frequency response of the output voltage of the ZnO sensor was obtained. Thicknesses of the ZnO thin film and overcoat were varied to study their effects on the sensor output.

4.1 Effect of ZnO thickness

Fig. 5 shows the response spectra with the basecoat thickness fixed at 20 μm. Regardless of the ZnO thickness, the peaks of the spectra all appear at 5.62 MHz,

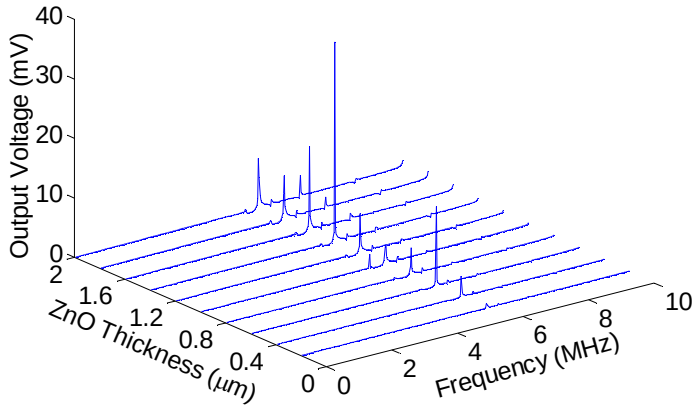

Fig. 5 Harmonic response spectra for overcoat thickness of 20 μm

which is slightly higher than the resonant frequency of the 2nd in-plane bending mode (5.52 MHz) as shown in Fig. 3(b). The difference is caused by the thickness of the overcoat. The overcoat thicknesses are 30 μm and 20 μm for the sliders in Fig. 3(b) and Fig. 5, respectively. Since the length of the slider remains 1.25 mm, the difference in the overcoat thickness is compensated by the slider body

material. As shown in Table 2, the Young's moudulus of the slider body material (Al_2O_3TiC) (390 GPa) is much higher than that of the overcoat material (Al_2O_3) (138 GPa). Therefore, the slider with 20 μm overcoat (Fig. 5) has a higher resonant frequency than the one with 30 μm overcoat (Fig 3(b)). Fig. 6 shows the output voltage induced by the 2nd in-plane bending mode. The output voltage overall increases with the ZnO thickness, however the voltage fluctuates in the process of trending upwards. The unparallel curves suggest that the ZnO thin film and base coat are not independent in terms of the effects of their thickness on the response.

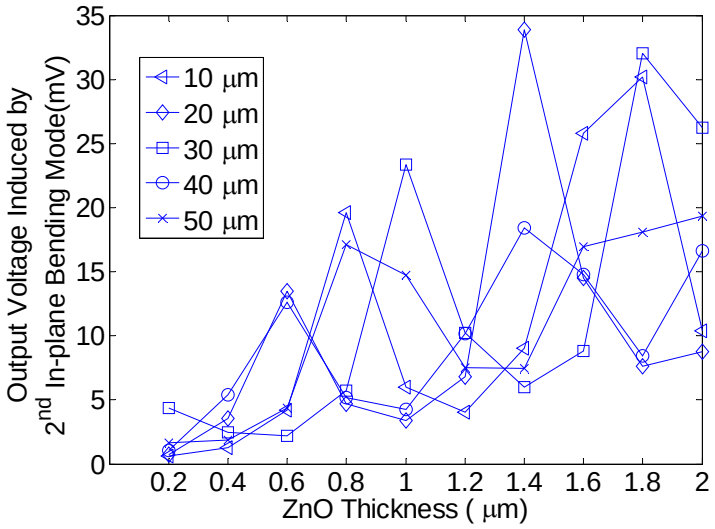

Fig. 6 Effect of ZnO thickness on output voltage

4.2 Effect of Overcoat thickness

The overcoat thickness was varied to study its effect on harmonic response of the sensor. Fig. 7 shows the response spectra with ZnO thickness set to 1 μm. The peaks again occur at the resonant frequencies of the 2nd bending mode. As explained earlier, the resonant frequency of the 2nd bending mode decreases with the overcoat thickness. As a result, the peak for 5 μm overcoat has the highest frequency (5.75 MHz), while the peak for 50 μm overcoat has the lowest frequency (5.375 MHz). In addition to the second bending mode, the 1st bending mode (5.15 MHz) is also observed in the spectra. The magnitudes of the peaks for the 1st bending mode are much smaller than those for the 2nd bending mode.

The highest peak for the 1st bending mode is 4.3 mV in contrast with 23.3 mV for the 2nd bending mode. It can be seen in Fig. 5 that only the spectrum with 1 μm ZnO has the 1st bending mode before the highest peak. This shows that the 1st bending mode is significant only for 1 μm ZnO thin film. The output voltage induced by the second bending mode is plotted against the overcoat thickness in Fig. 8. The effect of the basecoat thickness on the output voltage appears

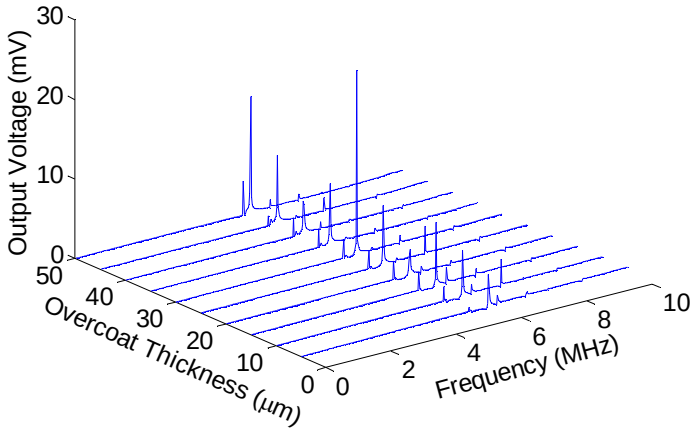

Fig. 7 Harmonic response spectra for ZnO thickness of 1 μm

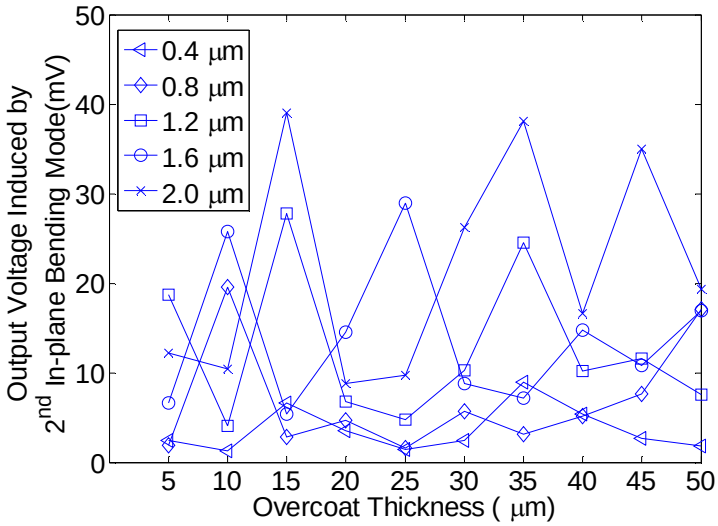

Fig. 8 Effect of overcoat thickness on output voltage

complicated because of the trade-off between strain and mass loading. In terms of maximizing strain, a thinner basecoat is preferred, as the ZnO thin film will be located closer to the surface. However, a thicker basecoat has the benefit of mass

loading on the ZnO layer. Comparing Fig. 6 and Fig. 8, it can be seen that in both cases there are significant fluctuations in the curves; however in Fig. 6 the curves overall rise up, while in Fig. 8 the curves appear flatter. Therefore, it can be concluded that the effect of ZnO thickness is greater than that of overcoat thickness.

4.3 Contributions of d_{31} and d_{33} modes

To investigate the contributions of d_{31} and d_{33} modes, the d_{33} and d_{31} constants were switched off accordingly in the piezoelectric strain matrix [**d**]. Fig. 9 shows the spectra of the output voltage for the two modes in comparison with a full [**d**]. It can be seen that the two curves for a full matrix [**d**] and $d_{33} = 0$ are almost overlapped, while the curve for $d_{31} = 0$ is significant lower. This reveals that the ZnO sensor dominantly operates in the d_{31} mode. The highest peak for a full matrix [**d**] and $d_{33} = 0$ is 21.5 mV at 5.52 MHz (2^{nd} bending mode), while for $d_{31} = 0$ the highest peak is 3.6 mV at 5.15 MHz (1^{st} bending mode). For $d_{31} = 0$, the peak still coincides with the first bending mode, even lateral strain does not contribute to output voltage directly. This phenomenon is caused mainly by strain coupling. Through coupling, lateral strain can induce normal strain which in turn generates voltage via the d_{33} mode.

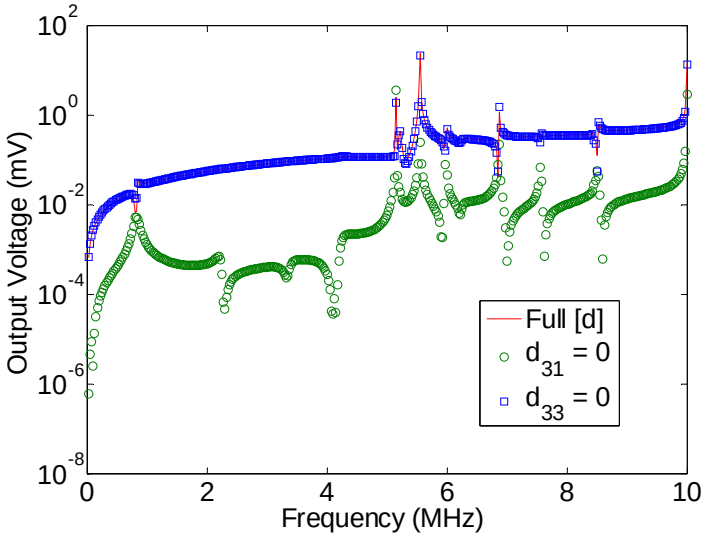

Fig. 9 Contributions of d_{31} and d_{33} modes

5 Transient analysis of sensor response

Three typical head-disk contact scenarios, i.e. a single contact, multiple contacts and continuous contact, were simulated in transient analysis. Time histories of the output voltage were obtained. The voltage amplitudes for all the three scenarios were in the range of milivolts.

5.1 Single head-disk contact

Fig. 10 shows time histories of the contact force, flying height deviation and output voltage for a single head-disk contact. As seen in Fig. 10(a), the contact force of 5 mN lasts 0.1 μs. Due to the impact, the flying height deviates instantly

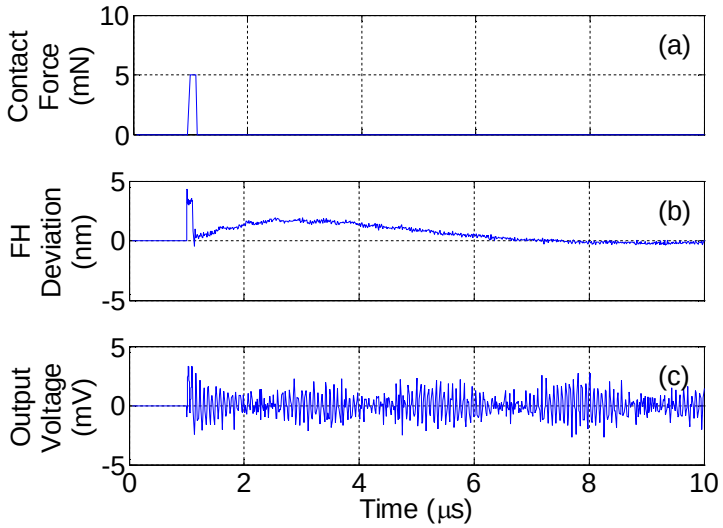

Fig. 10 A single head-disk contact: (a) contact force; (b) flying height deviation; (c) output voltage

by 4.5 nm and returns to the equilibrium position under damping from the air bearing (Fig. 10(b)). The output voltage shown in Fig. 10(c) rises up to 3.5 mV under the impact and decreases slightly during the ensuing free vibration.

5.2 Multiple head-disk contacts

In the second contact scenario, the slider collides with multiple bumps or protrusions on the disk. The induced contact force forms a pulse train (Fig. 11(a)). The magnitude and duration of the individual contact-force pulse are the same as those in a single contact. The time interval between two pulses is 1 μs. The contact forces generate repeating plateaus in the time history of flying height

deviation (Fig. 11(b)). Unlike in a single-contact scenario where the flying height returns to equilibrium, flying height deviation perturbed by multiple contacts remains at 5 nm after a contact in the pulse train. The voltage output is also higher than that in a single contact (Fig. 10(c)). The maximum voltage output for multiple head-disk contacts is 9.6 mV in the steady-state.

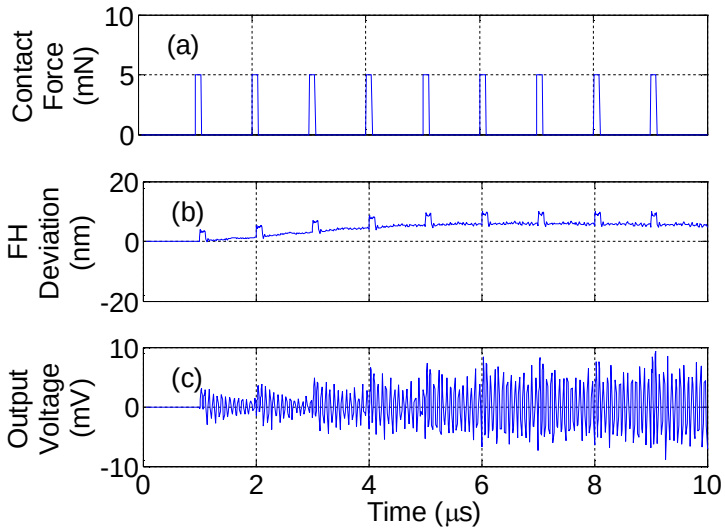

Fig.11 Multiple head-disk contacts: (a) contact force; (b) flying height deviation; (c) output voltage

5.3 Continuous head-disk contact

In the third contact scenario, the slider is in continuous contact with the disk. The contact force as seen in Fig. 12(a) is formed by superposition of four sinusoids with frequencies of 1 MHz, 4 MHz, 5.5 MHz and 7 MHz, respectively. Those frequencies originate from roughness and micro waviness of the disk surface (Gupta and Bogy 2008). For instance, with a wavelength of 3 μm and a rotational speed of 7200 rpm, when the slider is flying at a radius of 20 mm, the contact excitation frequency is calculated to be 5.03 MHz, close to the slider in-plane bending modes. To differentiate normal contact from adhesion, the force function is shifted upwards. The positive part represents the compressive force associated with normal contact, while the negative part simulates the tensile force attributed to adhesion. Fig. 12(b) shows that the flying height deviation reaches a steady state of 100 nm under continuous contact. And, due to the higher excitation

intensity, the output voltage increases to 20 mV which doubles from the multiple-contact scenario.

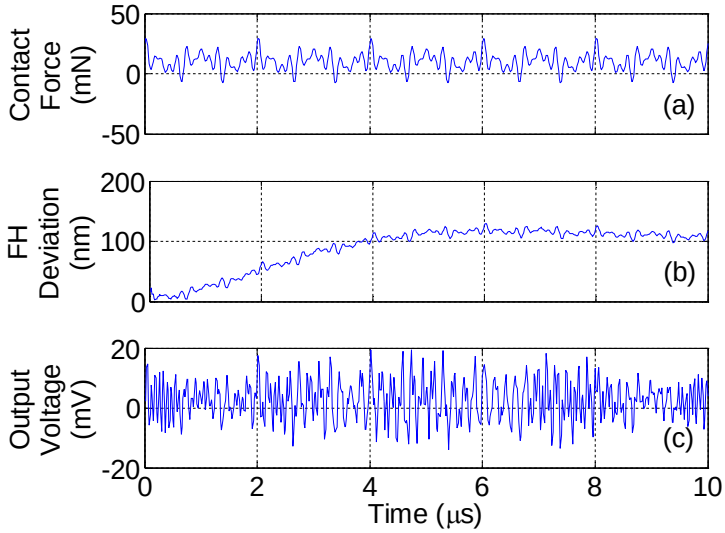

Fig. 12 Continuous head-disk contact: (a) contact force; (b) flying height deviation; (c) output voltage

6. Conclusions

The ZnO sensor for detection of head-disk contact is located on the trailing side of the slider and its fabrication is compatible with existing slider fabrication process. Modal, harmonic and transient analyses were performed to investigate the sensor response under typical head-disk contact scenarios. Under harmonic excitations, the output voltage ranges from under 5 mV to up to 35 mV depending on the thicknesses of the ZnO thin film and slider overcoat. The sensor operates dominantly on the d_{31} mode. The output voltage was generated mainly by lateral strain associated with the 2nd in-plane bending mode. Transient analysis showed that a single contact can generate a maximum sensor output of 3.5 mV, and under continuous contact the output voltage can reach up to 20 mV. The results showed that performance of the integrated piezoelectric ZnO sensor is adequate for detection of head-disk contact.

References

Allik H, Hughes TJR (1970) Finite element method for piezoelectric vibration. Int J Numer Methods Eng 2 (2):151-157. doi: 10.1002/nme.1620020202

Daugela A, Nagarajan S, Boutaghou ZE (2007) Ultra sensitive in-situ acoustic characterization system for HDD head disc interface defectoscopy. Microsyst Technol 13 (8-10):1185-1191. doi: 10.1007/s00542-006-0322-9

Gupta V, Bogy DB (2008) Optimal slider-disk surface topography for head-disk interface stability in hard disk drives. IEEE Trans Magn 44 (1):138-144. doi: 10.1109/Tmag.2007.911035

Collaboration (1988) IEEE standard on piezoelectricity. vol ANSI/IEEE Std 176-1987. Inst. Electr. & Electron. Eng., New York

Imai S, Burger GJ, Lammerink TSJ, Fluitman JHJ (1996) Fundamental study on a thin-film AE sensor for measurement of behavior of a multi-pad contact slider. IEEE Trans Magn 32 (5):3675-3677. doi: 10.1109/20.538725

Imai S, Tokuyama M, Hirose S, Burger GJ, Lammerink TSJ, Fluitman JHJ (1995) A thin-film piezoelectric impact sensor array fabricated on a Si slider for measuring head-disk interaction. IEEE Trans Magn 31 (6):3009-3011. doi: 10.1109/20.490253

Jagadish C, Pearton SJ (2006) Zinc oxide bulk, thin films and nanostructures : processing, properties and applications. Elsevier, Amsterdam ; Boston

Kita T, Kogure K, Mitsuya Y, Nakanishi T (1980) New method of detecting contact between floating-head and disk. IEEE Trans Magn. doi: 10.1109/TMAG.1980.1060719

Knigge B, Talke FE (2000) Contact force measurement using acoustic emission analysis and system identification methods. Tribol Int 33 (9):639-646. doi: 10.1016/S0301-679X(00)00080-3

Kohira H, Tanaka H, Matsumoto M, Talke FE (2001) Investigation of slider vibrations due to contact with a smooth disk surface. Trans ASME J Tribol 123 (3):616-623. doi:10.1115/1.1308045

Marchon B, Olson T (2009) Magnetic Spacing Trends: From LMR to PMR and Beyond. IEEE Trans Magn 45 (10):3608-3611. doi: 10.1109/Tmag.2009.2023624

Morkoç H, Özgür Ü (2009) Zinc oxide : fundamentals, materials and device technology. Wiley-VCH, Weinheim

Naniwa I, Sato K, Nakamura S, Sato K (2009) Active-head slider with piezoelectric actuator using shear-mode deformation. Microsyst Technol 15 (10-11):1619-1627. doi: 10.1007/s00542-009-0862-x

Shen S, Du H, Liu B, Wang P (2012) Simulation of thermal flying height control slider with built-in contact sensor. Microsyst Technol. doi:10.1007/s00542-012-1596-8

Wang S, Viswanathan KV, Liu HL (1998) Acoustic emission of laser textured disks influenced by bump excitation. IEEE Trans Magn 34 (4):1813-1815. doi: 10.1109/20.706715

Yeack-Scranton CE (1986) Novel piezoelectric transducers to monitor head-disk interactions. doi:10.1109/tmag.1986.1064624